Electrocatalysis

International Edition: DOI: 10.1002/anie.201506044
German Edition: DOI: 10.1002/ange.201506044

Photoelectron Spectroscopy at the Graphene–Liquid Interface Reveals the Electronic Structure of an Electrodeposited Cobalt/Graphene Electrocatalyst

Juan J. Velasco-Velez, Verena Pfeifer, Michael Hävecker, Robert S. Weatherup, Rosa Arrigo, Cheng-Hao Chuang, Eugen Stotz, Gisela Weinberg, Miquel Salmeron, Robert Schlögl, and Axel Knop-Gericke*

Abstract: *Electrochemically grown cobalt on graphene exhibits exceptional performance as a catalyst for the oxygen evolution reaction (OER) and provides the possibility of controlling the morphology and the chemical properties during deposition. However, the detailed atomic structure of this hybrid material is not well understood. To elucidate the Co/graphene electronic structure, we have developed a flow cell closed by a graphene membrane that provides electronic and chemical information on the active surfaces under atmospheric pressure and in the presence of liquids by means of X-ray photoelectron spectroscopy (XPS). We found that cobalt is anchored on graphene via carbonyl-like species, namely $Co(CO)_x$, promoting the reduction of Co^{3+} to Co^{2+}, which is believed to be the active site of the catalyst.*

Developing new clean energy-storage systems has become one of the most important challenges.[1] Electrolysis of water to produce hydrogen as a storable and clean fuel offers new opportunities to progressively replace the use of fossil fuels. Nevertheless, voltages well beyond the thermodynamic potential of 1.23 V are typically required to split water, mainly owing to the slow kinetics of the oxygen evolution reaction (OER) at the anode.[2] To achieve suitable current densities of at least 10 mA cm^{-2}, several hundred millivolts above the standard reaction potential are needed,[3] leading to poor process efficiencies. Metal oxides such as IrO_2 and RuO_2 and compounds thereof are the most active materials for the OER,[4] but these elements are expensive and among the rarest. Therefore, new catalysts based on abundant metal oxides and carbon-based materials have been developed.[5] Graphene has been found to be an ideal substrate for a wide range of energy-related applications,[6] in particular for electrocatalysis, becoming catalytically active through its functionalization with different materials.[7]

One noteworthy example is nanoscale Co grown on graphene. This system has demonstrated a remarkable performance in the OER and oxygen reduction reaction (ORR)[8] that is even better than that of C-based electrodes functionalized with noble-metal catalysts such as Pt[9] or Ir.[10] The functionalization of C with low-cost metals using electrochemical procedures opens up the possibility of controlling the morphology and chemical properties of the electrodeposited metal to increase its activity, selectivity, and corrosion resistance.[11] Thus far, the atomic structure and the interaction between Co and graphene as well as the nature of the active sites are not well understood. At present, the lack of experimental methods capable of providing atomic-level information on the electrochemical processes occurring at the solid/liquid interfaces remains a major obstacle to the improvement of these catalysts.

Advances such as (near-)ambient-pressure photoelectron spectroscopy (NAP-XPS)[12] have enabled the study of liquids under vapor pressures in the mbar range compared to previous studies in UHV. Recently, electrochemical cells based on a proton exchange membrane have been developed,[13] making it possible to investigate the electronic structure of Pt and Ir anodes during the OER under low water vapor pressures. Another promising approach combines X-ray absorption spectroscopy (XAS) in the total electron yield mode (TEY) with a frequency discrimination method using X-ray beam intensity modulation and lock-in-amplifier detection and enables the investigation of the structure of water close to a gold surface under an applied bias.[14] Recently, a method based on the preparation of nanometer-thin liquid films at the tail of a wetting meniscus that is formed in an electrode partially immersed in the electrolyte has been developed,[15] which requires X-rays of

[*] Dr. J. J. Velasco-Velez, Dr. M. Hävecker, Prof. Dr. R. Schlögl
Max Planck Institute for Chemical Energy Conversion
Mülheim 45470 (Germany)
E-mail: velasco@fhi-berlin.mpg.de
Dr. J. J. Velasco-Velez, V. Pfeifer, E. Stotz, G. Weinberg, Prof. Dr. R. Schlögl, Dr. A. Knop-Gericke
Fritz-Haber-Institut der Max-Planck-Gesellschaft
Berlin 14195 (Germany)
Dr. M. Hävecker
Helmholtz-Center Berlin for Materials and Energy, BESSY II
Berlin 12489 (Germany)
Dr. R. S. Weatherup
Engineering Department, University of Cambridge
Cambridge CB3 0FA (UK)
Dr. R. S. Weatherup, Prof. Dr. M. Salmeron
Materials Science Division
Lawrence Berkeley National Laboratory
Berkeley 94720 (USA)
Dr. R. Arrigo
Diamond Light Source
Oxfordshire OX11 0QX (UK)
Prof. Dr. C.-H. Chuang
Department of Physics, Tamkang University
Tamsui 251 (Taiwan)

Supporting information for this article is available on the WWW under http://dx.doi.org/10.1002/anie.201506044.

several keV to allow photoelectrons to escape through the thin liquid film.

A different approach entails the use of an electron-transparent membrane based on graphene to separate the vacuum measurement chamber from a cell filled with liquid.[16] The X-rays can easily penetrate the mono- or bilayer graphene film, and photoelectrons can escape and be detected on the vacuum side. Based on this idea, we constructed an electrochemical liquid flow cell with a bilayer graphene (BLG) membrane following the procedure described in the Supporting Information.[17] Figure 1 shows

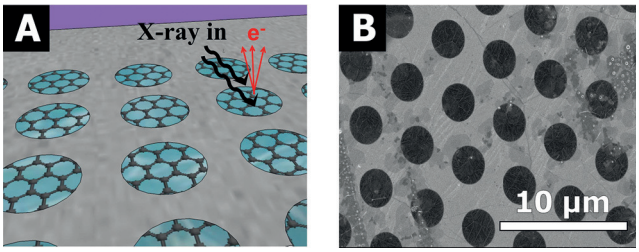

Figure 1. A) Schematic representation of the Si_3N_4 grid coated with bilayer graphene (BLG). The incoming X-ray produces two kinds of signals: photons from core–hole decay and Auger/photoelectrons. B) SEM image of a Si_3N_4 grid with an array covered by BLG.

a schematic drawing of the grid of holes coated with graphene and a corresponding scanning electron microscopy (SEM) image (the full membrane is shown in the Supporting Information, Figure S2). This cell allows us to detect photo- and Auger electrons generated near the solid/liquid interface. Furthermore, XAS can be performed in TEY and fluorescence yield (FY) modes. The liquid flow cell (Figure S3) is operated inside the main chamber of the ISISS[18] end station at the synchrotron radiation source BESSY II at a pressure of approximately 10^{-7} mbar while aqueous solutions circulate on the back side of the membrane. Technical details are described in the Supporting Information.

To produce catalytically active Co/graphene composites, a 4 mM $CoSO_4$ solution prepared with ultrapure Milli-Q water was passed through our cell, and we performed an underpotential deposition as described in Figure 2. This method

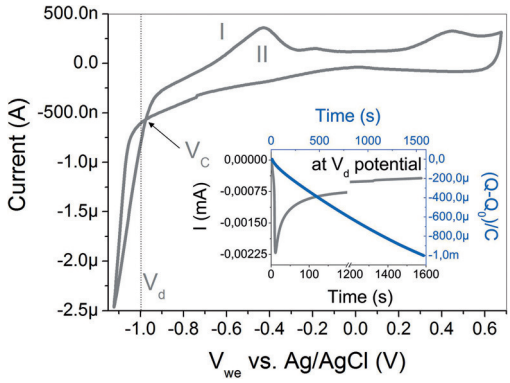

Figure 2. Cyclic voltammogram and charge-transfer curve (inset) at −1 V in 4 mM $CoSO_4$ electrolyte.

allows us to electrochemically control the deposition rate and the oxidation state. The complex reaction process involves several steps, such as diffusion of electroactive species, desolvation, formation, and incorporation of ad-atoms at lattice sites of the growing deposit.

Figure 2 shows a cyclic voltammogram (CV) recorded at 20 mV s^{-1}. The cross-potential (V_C) at −0.9 V corresponds to the equilibrium potential of the metal redox couple (Co^{2+}/Co^0).[19] The maxima I and II are associated with the dissolution of deposited Co or with the oxidation of two different Co phases.[20] The inset of Figure 2 shows a chronoamperogram (CA) and the total charge transferred during electrodeposition at a deposition voltage (V_d) of −1.0 V. The total charge transferred was 1 mC after about 1600 s. The thickness of the electrodeposited Co can thus be estimated according to:

$$x = \frac{M \cdot Q_T}{\rho \cdot A \cdot n \cdot F},$$

where M = molar mass, Q_T = total charge transferred, ρ = density, A = effective area, n = valence of the metal, and F = Faraday's constant. The electrodeposited film was probed with SEM and energy-dispersive X-ray spectroscopy (EDX) from the side that had been exposed to the UHV (see Figure 3). The images show that Co (magenta) has been deposited across the graphene membrane as all graphene-covered holes show a relatively homogeneous Co coverage.

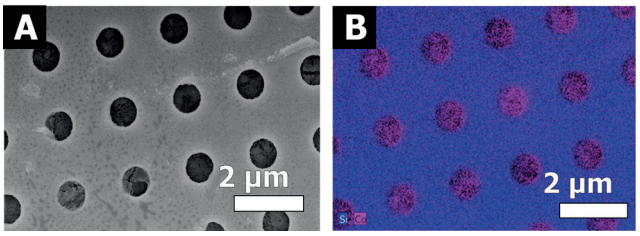

Figure 3. A) SEM image of the membrane and B) Co/Si EDX mapping on the back side, UHV interface (Co magenta, Si blue).

The OER activity of the Co electrodeposited onto graphene was evaluated with a 10 mM KOH solution. Figure 4a shows the CVs (recorded at 20 mV s^{-1}) of pristine graphene and the Co/graphene electrodes. For the electrodeposited Co, the CV shows two oxidation peaks and one reduction peak.[21] The anodic peaks observed at about 0.6 V (I) and 1.2 V (II) are ascribed to the oxidation of Co^{2+} to Co^{3+} and Co^{3+} to Co^{4+}, respectively. The peak at approximately 1.1 V (III) is assigned to the transition from Co^{4+} to Co^{2+} when the potential is reversed, indicating that the OER is preceded by Co oxidation. Furthermore, the OER was analyzed by linear sweep voltammetry (LSV) at a scan rate of 20 mV s^{-1} (see Figure 4b). A noteworthy overpotential decrease that is due to the presence of Co is seen, which was evaluated at a current density of 10 mA cm^{-2}.

The electronic structure of the Co electrodeposited onto graphene was investigated by means of X-ray spectroscopy.

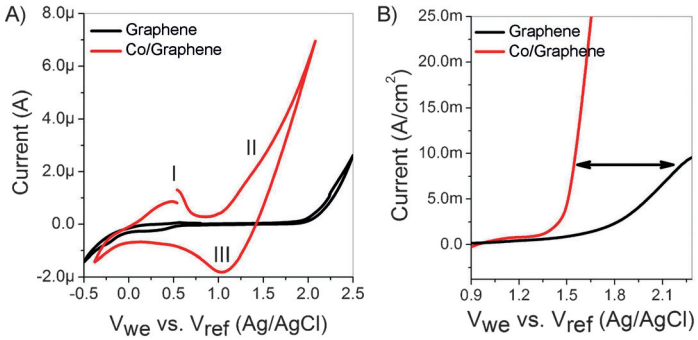

Figure 4. A) CV and B) LSV of pristine graphene and Co electrodeposited on graphene. The measurements were performed in 10 mM KOH using a three-electrode cell with a Pt counter electrode and a Ag/AgCl reference electrode.

Accordingly, the in situ XAS measurements were conducted under operating conditions. The Co $L_{3,2}$ edges involve excitation of the 2p electrons to the unoccupied Co 3d states and are sensitive to the valence and the coordination environment of the Co atoms.[22] Figure 5a shows the XA spectra recorded before and during the electrodeposition of Co, which were recorded in TEY mode (lower panel, red spectra) from the photoelectrons emitted through the graphene membrane outside the cell and in FY mode (top panel, green spectra) by the photons emitted. The TEY mode is more sensitive to the layers near the Co/graphene interface owing to the short inelastic mean free path of electrons in solids whereas the FY mode is mostly bulk-sensitive because of the larger photon penetration depth. Therefore, the combination of these two modes provides insights concerning the anchoring between Co and graphene as well as details of the bulk chemical state. During electrodeposition, the TEY signal for the Co L edge is consistent with the rock-salt CoO structure, with an intense peak at 777.4 eV associated with Co^{2+}.[23] Meanwhile, the FY spectrum is characteristic of Co_3O_4, as indicated by the intense Co^{3+} peak at 780.2 eV. Consequently, the anchoring of Co onto graphene prompts the reduction from Co^{3+} (bulk) to Co^{2+} (interface), which is associated with the substitution of O ligands by C in Co_3O_4 in the form of $Co(CO)_x$.

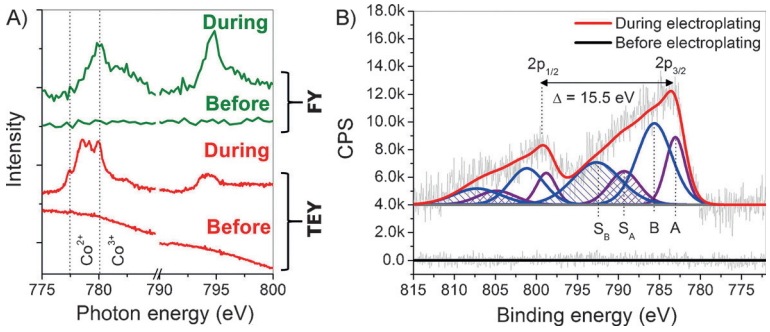

Figure 5. A) XAS Co L-edge collected in TEY mode (lower panel, red spectra) before and during electroplating and in FY mode (upper panel, green spectra). B) Co 2p XPS region before (bottom, black curve) and during electroplating (top, red curve).

Furthermore, the electronic structure was investigated with XPS, which probes the core-level binding energies of the constituent species. Figure 5b shows the Co 2p XPS region collected before and during the Co electroplating process. The Co 2p spectra feature a doublet $2p_{3/2}$ and $2p_{1/2}$ with a spin–orbit splitting of $\Delta E = 15.5$ eV. Peak assignment and species quantification are challenging as most of the species appear within a 2.5 eV binding energy (BE) range, including the complex satellite structure characteristic of first-row transition metals,[24] which is indicative of Co^{2+}/Co^{3+} with unpaired d electrons and could be associated with an oxygen-rich environment. Therefore, some ambiguity in the peak assignment and the quantification of such components still exists owing to species with similar BEs resulting in overlapping peaks for adjacent species.[25] It has been suggested that the XPS 2p peak deconvolution of transition-metal species cannot be done using a single-peak approach owing to multiplet splitting and the satellite structure.[26] The close interaction of C with Co can be compared to a previous XPS investigation of pristine and deposited cobaltocene films.[27] In this investigation, the pure cobaltocene film showed two main peaks at binding energies of approximately 783 eV and 798 eV, which correspond to the spin–orbit split Co $2p_{3/2}$ and Co $2p_{1/2}$ components and are in good agreement with our measurements. Accordingly, the Co $2p_{3/2}$ spectrum here was deconvoluted using two dominant Gaussian–Lorentzian peaks at binding energies of 783.2 eV (peak A) and 785.6 eV (peak B) with two shake-up satellites at 6 eV higher BEs than the main peaks (S_A and S_B). The Co $2p_{3/2}$/Co $2p_{1/2}$ intensity ratio was fixed to 2. The peak at about 783.2 eV (peak A) has typically been attributed to Co^{2+}.[28] Therefore, Co^{2+} bound to C appears responsible for the peak observed here at this same BE, which shows multiplet splitting and a satellite structure and is responsible for the majority of the signal seen. Small amounts of $Co_xO_y(OH)_z$ may also be present and contribute to the Co 2p spectrum.[29] Furthermore, the peaks at 783.2 eV (peak A) and 785.6 eV (peak B) can also be related to the formation of Co bound to oxygen in the form of carbonyl-like species such as $Co(CO)_x$,[24,30] as a comparison with pyrolyzed and porphyrin Co samples reveals. The higher-binding-energy regions of these peaks overlap with the shake-up satellite envelopes S_A and S_B,[26,31] which are associated with the presence of Co^{2+} species. Consequently, the synergistic interaction between Co and graphene has been probed, which reveals that the anchoring of Co to the graphene by means of $Co(CO)_x$ bonds yields Co^{2+} species.

In summary, the anchoring and chemical state of electrodeposited Co on a graphene electrode and its OER electrochemical activity have been investigated under operando conditions. This analysis was made feasible by the development of a novel electrochemical cell that entails an electron-transparent membrane based on bilayer graphene, which facilitates electron spectroscopy at electrode–electrolyte interfaces with potentiometric control. Using this approach,

we have demonstrated that the electrodeposition of Co onto graphene leads to the reduction of Co^{3+} to Co^{2+} species at the interface. The anchoring of Co on graphene is due to the formation of Co bound to oxygen in the form of $Co(CO)_x$ species. Therefore, the enhancements in electrocatalytic activity and stability shown by Co/Graphene composites in the OER are likely related to the hybrid interface contacts, which control and promote the electron transfer reactions. The increase in the catalytic activity as well as the binding mechanism of the Co oxide catalyst are attributed to Co^{2+} active sites derived from the reduction of Co^{3+} species. This novel setup opens the way for studies of electrode processes with high sensitivity to the interfaces, both with surface-sensitive electron spectroscopy and electron-microscopy-based techniques.

Acknowledgements

We thank the staff at BESSY II of the HZB for operational support, the HZB for providing beam time at the ISISS end station (proposal 14201159), Philipp Braeuninger-Weimer for providing CVD graphene on Cu foil, and Stephan Hofmann for useful discussions. This work was financially supported through the following agencies and grants: EU project GRAFOL (285275), the Ministry of Education and Science of the Russian Federation (14.616.21.0007) and the Bundesministerium für Bildung und Forschung (05K2014) through the joint Russian–German research project "SYnchrotron and NEutron STudies for Energy Storage" (SYNESTESia), St. John's College, Cambridge (Research Fellowship to R.S.W.), a Marie Skłodowska-Curie Individual Fellowship (Global; ARTIST programme, 656870) from the European Union's Horizon 2020 research and innovation programme, the projects 103-2112-M-032-004 and 102-2632-M-032-001-MY3 (C.H.C.), and the Office of Science, Division of Materials Sciences and Engineering of the U.S. Department of Energy (DOE; DE-AC02-05CH11231, M.S.).

Keywords: electrocatalysis · electrodeposition · graphene/cobalt · photoelectron spectroscopy · X-ray absorption spectroscopy

How to cite: *Angew. Chem. Int. Ed.* **2015**, *54*, 14554–14558
Angew. Chem. **2015**, *127*, 14762–14766

[1] J. Chow, R. J. Kopp, P. R. Portney, *Science* **2003**, *302*, 1528–1531.
[2] M. G. Walter, E. L. Warren, J. R. McKone, S. W. Boettcher, Q. Mi, E. A. Santori, N. S. Lewis, *Chem. Rev.* **2010**, *110*, 6446–6473.
[3] a) K. Gong, F. Du, Z. Xia, M. Durstock, L. Dai, *Science* **2009**, *323*, 760–764; b) Y. Gorlin, T. F. Jaramillo, *J. Am. Chem. Soc.* **2010**, *132*, 13612–13614.
[4] a) Y. Lee, J. Suntivich, K. J. May, E. E. Perry, Y. Shao-Horn, *J. Phys. Chem. Lett.* **2012**, *3*, 399–404; b) T. C. Wen, C. C. Hu, *J. Electrochem. Soc.* **1992**, *139*, 2158–2163.
[5] a) I. V. Lightcap, T. H. Kosel, P. V. Kamat, *Nano Lett.* **2010**, *10*, 577–583; b) P. V. Kamat, *J. Phys. Chem. Lett.* **2010**, *1*, 520–527.
[6] a) S. Bai, X. Shen, *RSC Adv.* **2012**, *2*, 64–98; b) B. F. Machado, P. Serp, *Catal. Sci. Technol.* **2012**, *2*, 54–75; c) S. Bose, T. Kuila, A. K. Mishra, R. Rajasekar, N. H. Kim, J. H. Lee, *J. Mater. Chem.* **2012**, *22*, 767–784.
[7] a) Z. S. Wu, G. Zhou, L. C. Yin, W. Ren, F. Li, H. M. Cheng, *Nano Energy* **2012**, *1*, 107–131; b) Y. Liang, Y. Li, H. Wang, J. Zhou, J. Wang, T. Regier, H. Dai, *Nat. Mater.* **2011**, *10*, 780–786.
[8] S. Mao, Z. Wen, T. Huang, Y. Hou, J. Cheng, *Energy Environ. Sci.* **2014**, *7*, 609–616.
[9] J. Wang, J. Zhou, Y. Hu, T. Regier, *Energy Environ. Sci.* **2013**, *6*, 926–934.
[10] L. Wu, C. H. Wu, H. Zhu, A. Mendoza-Garcia, B. Shen, J. Guo, S. Sun, *J. Am. Chem. Soc.* **2015**, *137*, 7071–7074.
[11] B. Bozzini, P. Bocchetta, A. Gionancelli, C. Mele, M. Kiskinova, *Acta Chim. Slov.* **2014**, *61*, 263–271.
[12] a) M. Salmeron, R. Schlögl, *Surf. Sci. Rep.* **2008**, *63*, 169–199; b) D. E. Starr, Z. Liu, M. Hävecker, A. Knop-Gericke, H. Bluhm, *Chem. Soc. Rev.* **2013**, *42*, 5833–5857.
[13] a) R. Arrigo, M. E. Schuster, C. Ranjan, E. Stotz, A. Knop-Gericke, R. Schlögl, *Angew. Chem. Int. Ed.* **2013**, *52*, 11660–11664; *Angew. Chem.* **2013**, *125*, 11874–11879; b) H. S. Casalongue, S. Kaya, V. Viswanathan, D. J. Miller, D. Friebel, H. A. Hansen, J. K. Nørskov, A. Nilsson, H. Ogasawara, *Nat. Commun.* **2013**, *4*, 2817; c) H. S. Casalongue, M. L. Ng, S. Kaya, D. Friebel, H. Ogasawara, A Nilsson, *Angew. Chem. Int. Ed.* **2014**, *53*, 7169–7172; *Angew. Chem.* **2014**, *126*, 7297–7300.
[14] J. J. Velasco-Velez, C. H. Wu, T. A. Pascal, L. F. Wan, J. Guo, D. Prendergast, M. Salmeron, *Science* **2014**, *346*, 831–834.
[15] a) O. Karslioglu et al., *Faraday Discuss.* **2015**, *180*, 35–53; b) S. Nemšak et al., *Nat. Commun.* **2014**, *5*, 5441.
[16] A. Kolmakov, D. A. Dikin, L. J. Cote, J. Huang, M. K. Abyaneh, M. Amati, L. Gregoratti, S. Günter, M. Kiskinova, *Nat. Nanotechnol.* **2011**, *6*, 651–657.
[17] a) R. S. Weatherup, B. Dlubak, S. Hofmann, *ACS Nano* **2012**, *6*, 9996–10003; b) P. R. Kidambi, C. Ducati, B. Dlubak, D. Gardiner, R. S. Weatherup, M. B. Martin, P. Seneor, H. Coles, S. Hofmann, *J. Phys. Chem. C* **2012**, *116*, 22492–22501; c) J. J. Velasco-Velez, C. H. Wu, B. Y. Wang, Y. Sun, Y. Zhang, J. H. Guo, M. Salmeron, *J. Phys. Chem. C* **2014**, *118*, 25456–25459; d) J. J. Velasco-Velez, C. H. Chuang, H. L. Han, I. Martinez-Fernandez, C. Martinez, W. F. Pong, Y. R. Shen, F. Wang, Y. Zhang, J. Guo, M. Salmeron, *J. Electrochem. Soc.* **2013**, *160*, C445–C450; e) S. Hofmann, P. Braeuninger-Weimer, R. S. Weatherup, *J. Phys. Chem. Lett.* **2015**, *6*, 2714–2721.
[18] A. Knop-Gericke et al., *Adv. Catal.* **2009**, *52*, 213–272.
[19] S. Fletcher, *Electrochim. Acta* **1983**, *28*, 817–923.
[20] M. Palomar-Pardavé, I. González, A. B. Soto, E. M. Arce, *Electroanal. Chem.* **1998**, *443*, 125–136.
[21] J. Ismail, M. F. Ahmed, P. V. Kamath, *J. Power Sources* **1991**, *36*, 507–516.
[22] Y. Liang et al., *J. Am. Chem. Soc.* **2012**, *134*, 15849–15857.
[23] Q. He, Q. Li, S. Khene, X. Ren, F. E. Lopez-Suarez, D. Lozano-Castello, A. Bueno-Lopez, G. Wu, *J. Phys. Chem. C* **2013**, *117*, 8697–8707.
[24] J. J. Pietron, J. C. Biffinger, S. B. Qadri, D. R. Rolison, *J. Mater. Chem.* **2011**, *21*, 7668–7677.
[25] K. Artyushkova, S. Levendosky, J. Fulghum, P. Aanassov, *Top. Catal.* **2007**, *46*, 263–275.
[26] M. C. Biesinger, B. P. Payna, A. P. Grosvenor, L. W. M. Lau, A. R. Gerson, R. St. C. Smart, *Appl. Surf. Sci.* **2011**, *257*, 2717–2730.
[27] C. K. Chan, A. Kahn, Q. Zhang, S. Barlow, S. R. Marder, *Appl. Phys.* **2007**, *102*, 014906.
[28] a) X. Xiang, L. Zhang, H. I. Hima, F. Li, D. G. Evans, *Appl. Clay Sci.* **2009**, *42*, 405–409; b) V. Musat, E. Fortunato, A. M. B. Do Rego, R. Monteiro, *Thin Solid Films* **2008**, *516*, 1499–1502; c) R. S. Da Cruz, A. J. S. Mascarenhas, H. M. C. Andrade, *Appl. Catal. B* **1998**, *18*, 223–231.
[29] a) S. Cobo et al., *Nat. Mater.* **2012**, *11*, 802–807; b) R. Xu, H. C. Zeng, *Chem. Mater.* **2003**, *15*, 2040–2048.

[30] a) K. Artyushkova, S. Pylypenko, T. S. Olson, J. E. Fulghum, P. Atanasov, *Langmuir* **2008**, *24*, 9082 – 9088; b) S. Pylypenko, S. Mukherjee, T. S. Olson, P. Atanassov, *Electrochim. Acta* **2008**, *53*, 7875 – 7883; c) T. S. Olson, S. Pylypenko, P. Atanassov, K. Yamada, H. Tanaka, *J. Phys. Chem. C* **2010**, *114*, 5049 – 5059.

[31] M. Hu, Y. Murakami, M. Ogura, S. Maruyama, T. Okubo, *J. Catal.* **2004**, *225*, 230 – 239.

Received: July 1, 2015
Revised: July 17, 2015
Published online: October 14, 2015

